A simplified approach to quantitative coded aperture X-ray phase imaging

Peter R.T. Munro,[1,2,*] **Charlotte K. Hagen,**[3] **Magdalena B. Szafraniec,**[3] **and Alessandro Olivo**[3]

[1]*Optical + Biomedical Engineering Laboratory, School of Electrical, Electronic and Computer Engineering, The University of Western Australia, 35 Stirling Highway, Crawley, Western Australia 6009, Australia*

[2]*Centre for Microscopy, Characterisation and Analysis, The University of Western Australia, 35 Stirling Highway, Crawley, Western Australia, 6009, Australia*

[3]*Department of Medical Physics and Bioengineering, University College London, Malet Place, Gower Street, London WC1E 6BT, UK*

[*]*peter.munro@uwa.edu.au*

Abstract: We recently demonstrated how quantitative X-ray phase contrast imaging may be performed with laboratory sources using the coded aperture technique. This technique required the knowledge of system parameters such as, for example, the source focal spot size and distances between elements of the imaging system. The method also assumes that the absorbing regions of the apertures are perfectly absorbing. In this paper we demonstrate how quantitative imaging can be performed without knowledge of individual system parameters and with partially absorbing apertures. We also show that this method is analogous to that employed in analyser based imaging which uses the rocking curve of an analyser crystal.

OCIS codes: (110.7440) X-ray imaging;(120.5050) Phase measurement.

References and links

1. A. Olivo and R. Speller, "A coded-aperture technique allowing x-ray phase contrast imaging with conventional sources," Appl. Phys. Lett. **91**, 074106 (2007).
2. T. Davis, D. Gao, T. Gureyev, A. Stevenson, and S. Wilkins, "Phase-contrast imaging of weakly absorbing materials using hard x-rays," Nature **373**, 595–598 (1995).
3. D. Chapman, W. Thomlinson, F. Arfelli, N. Gmür, Z. Zhong, R. Menk, R. E. Johnson, D. Washburn, E. Pisano, and D. Sayers, "Mammography imaging studies using a laue crystal analyzer," The 9th National Conference on Synchrotron Radiation Instrumentation **67**, 3360–3360 (1996).
4. D. Chapman, W. Thomlinson, R. Johnston, D. Washburn, E. Pisano, N. Gmür, Z. . Zhong, R. Menk, F. Arfelli, and D. Sayers, "Diffraction enhanced x-ray imaging," Phys. Med. Biol. **42**, 2015–2025 (1997).
5. D. Paganin, T. E. Gureyev, K. M. Pavlov, R. A. Lewis, and M. Kitchen, "Phase retrieval using coherent imaging systems with linear transfer functions," Opt. Commun. **234**, 87–105 (2004).
6. Y. I. Nesterets, T. Gureyev, D. Paganin, K. Pavlov, and S. W. Wilkins, "Quantitative diffraction-enhanced x-ray imaging of weak objects," J. Phys. D Appl. Phys. **37**, 1262–1274 (2004).
7. M. J. Kitchen, D. M. Paganin, K. Uesugi, B. J. Allison, R. A. Lewis, S. B. Hooper, and K. M. Pavlov, "X-ray phase, absorption and scatter retrieval using two or more phase contrast images," Opt. Express **18**, 19994–20012 (2010).
8. P. C. Diemoz, P. Coan, C. Glaser, and A. Bravin, "Absorption, refraction and scattering in analyzer-based imaging: comparison of different algorithms," Opt. Express **18**, 3494–3509 (2010).
9. D. J. Vine, D. M. Paganin, K. M. Pavlov, J. Kraeusslich, O. Wehrhan, I. Uschmann, and E. Foerster, "Analyzer-based phase contrast imaging and phase retrieval using a rotating anode x-ray source," Appl. Phys. Lett. **91**, 254110 (2007).
10. C. Kottler, F. Pfeiffer, O. Bunk, C. Gruenzweig, J. Bruder, R. Kaufmann, L. Tlustos, H. Walt, I. Briod, T. Weitkamp, and C. David, "Phase contrast x-ray imaging of large samples using an incoherent laboratory source," Phys. Status Solidi. A **204**, 2728–2733 (2007).

#181390 - $15.00 USD Received 7 Dec 2012; revised 11 Mar 2013; accepted 16 Mar 2013; published 30 Apr 2013

11. F. Pfeiffer, T. Weitkamp, O. Bunk, and C. David, "Phase retrieval and differential phase-contrast imaging with low-brilliance x-ray sources," Nat. Phys. **2**, 258–261 (2006).
12. A. Momose, W. Yashiro, H. Kuwabara, and K. Kawabata, "Grating-based x-ray phase imaging using multiline x-ray source," Jpn. J. Appl. Phys. **48**, 076512 (2009).
13. A. Momose, "Recent advances in x-ray phase imaging," Jpn. J. Appl. Phys. **44**, 6355–6367 (2005).
14. A. Olivo, F. Arfelli, G. Cantatore, R. Longo, R. Menk, S. Pani, M. Prest, P. Poropat, L. Rigon, G. Tromba, E. Vallazza, and E. Castelli, "An innovative digital imaging set-up allowing a low-dose approach to phase contrast applications in the medical field," Med. Phys. **28**, 1610–1619 (2001).
15. P. Munro, K. Ignatyev, R. Speller, and A. Olivo, "Phase and absorption retrieval using incoherent x-ray sources," Proc. Natl. Acad. Sci. USA **109**, 13922–13927 (2012).
16. P. R. Munro, L. Rigon, K. Ignatyev, F. C. Lopez, D. Dreossi, R. D. Speller, and A. Olivo, "A quantitative, non-interferometric x-ray phase contrast imaging technique," Opt. Express **21**, 647–661 (2013).
17. P. Munro, K. Ignatyev, R. Speller, and A. Olivo, "Source size and temporal coherence requirements of coded aperture type x-ray phase contrast imaging systems," Opt. Express **18**, 19681–19692 (2010).
18. M. Marenzana, C. K. Hagen, P. D. N. Borges, M. Endrizzi, M. B. Szafraniec, K. Ignatyev, and A. Olivo, "Visualization of small lesions in rat cartilage by means of laboratory-based x-ray phase contrast imaging," Phys. Med. Biol. **57**, 8173–8184 (2012).
19. S. Mayo, P. Miller, S. Wilkins, T. Davis, D. Gao, T. Gureyev, D. Paganin, D. Parry, A. Pogany, and A. Stevenson, "Quantitative x-ray projection microscopy: phase-contrast and multi-spectral imaging," Journal of Microscopy-Oxford **207**, 79–96 (2002).
20. T. Gureyev and S. Wilkins, "On x-ray phase imaging with a point source," J. Opt. Soc. Am. A **15**, 579–585 (1998).
21. D. Paganin, *Coherent X-ray optics*, Oxford series on synchrotron radiation (Oxford University Press, Great Clarendon Street, Oxford OX2 6DP, 2006).
22. P. Munro, K. Ignatyev, R. Speller, and A. Olivo, "The relationship between wave and geometrical optics models of coded aperture type x-ray phase contrast imaging systems," Opt. Express **18**, 4103–4117 (2010).
23. A. Olivo and R. Speller, "Experimental validation of a simple model capable of predicting the phase contrast imaging capabilities of any x-ray imaging system," Phys. Med. Biol. **51**, 3015–3030 (2006).
24. P. C. Diemoz, P. Coan, I. Zanette, A. Bravin, S. Lang, C. Glaser, and T. Weitkamp, "A simplified approach for computed tomography with an x-ray grating interferometer," Opt. Express **19**, 1691–1698 (2011).
25. M. Chabior, T. Donath, C. David, O. Bunk, M. Schuster, C. Schroer, and F. Pfeiffer, "Beam hardening effects in grating-based x-ray phase-contrast imaging," Med. Phys. **38**, 1189–1195 (2011).
26. B. Henke, E. Gullikson, and J. Davis, "X-ray interactions: Photoabsorption, scattering, transmission, and reflection at e = 50-30,000 ev, z = 1-92," Atom. Data Nucl. Data **54**, 181–342 (1993).

1. Introduction

Coded aperture X-ray phase contrast imaging (CAXPCI) [1] was initially inspired by the synchrotron method known as analyser based imaging (ABI). ABI develops contrast using the rocking curve of an analyser crystal [2]. Algorithms were developed to extract sample phase and absorption from images taken on two opposing sides of the analyser crystal rocking curve [3,4]. Algorithms employing a variety of assumptions about the sample and imaging system, and later, for more general systems were subsequently developed [5–8]. Although this technique has been demonstrated using a laboratory source [9], it is generally restricted to synchrotron sources due to the narrow band of energies selected by the two crystals employed in the imaging system.

The restriction to synchrotron sources for applications not compatible with long exposure times motivated several people to develop alternative methods of performing X-ray phase contrast imaging (XPCI) using laboratory sources [1, 10–12]. It is beyond the scope of this paper to review the substantial number of contributions to this field, however we direct readers to a review on the subject [13] for such an account. One such contribution resulted from initial experiments performed using the SYRMEP beamline of the Elettra synchrotron radiation facility in operation in Trieste [14], an experiment directly inspired by analyser based imaging. Although initially demonstrated using synchrotron radiation, the technique was soon demonstrated using laboratory sources [1]. Recently this technique has been extended to a quantitative method for both laboratory [15] and synchrotron sources [16].

The CAXPCI system is schematised in Fig. 1(a) where all parameters are defined in the fig-

#181390 - $15.00 USD Received 7 Dec 2012; revised 11 Mar 2013; accepted 16 Mar 2013; published 30 Apr 2013

ure caption. Phase contrast images are obtained by adjusting the position of A_1 with respect to A_2 such that the beams formed by A_1 illuminate the edges of the A_2. A_2 is initially aligned with the detector pixels and remains stationary thereafter. Higher resolution images may be obtained by scanning the sample in the ξ direction as indicated in Fig. 1(b). CAXPCI imaging can be performed with synchrotron radiation [16] or laboratory sources [15]. The is no limit on the spectral width of the source so long as the apertures are thick enough to generate contrast in the detected signal, in the absence of a sample, which exceeds the noise. The focal spot size should not exceed the pixel size of the detector [17]. The system has recently been shown to have sensitivity which is at least comparable to that of grating interferometry [18], the only other system to offer high phase sensitivity when employing a laboratory source. The difference between grating interferometry and CAXPCI has been discussed in detail previously [17]. However, we note that the main difference is that CAXPCI employs the edge illumination principle where the edges of the sensitive region of a pixel are illuminated by X-ray beams. This means that CAXPCI doesn't make use of Talbot's self-imaging phenomenon and doesn't employ phase stepping of the detector aperture.

The existing quantitative method [15] was developed from a wave optical model of the CAXPCI system which took into account the principal system parameters such as source focal spot size and aperture dimensions and spacing. This technique thus requires such system parameters to be known to a reasonable degree of accuracy. However, some system parameters such as, for example, the source focal spot and spectrum are difficult to measure on a regular basis. It would be much more convenient if the effect of all system parameters could be aggregated into a single series of measurements, thus forming a simple method of calibrating the imaging system. We present such a method in this paper whereby a measurement, analogous to the rocking curve in ABI, is performed which forms the basis of the algorithm used to obtain quantitative phase measurements. We shall call this measurement the translation curve (TC) in order to distinguish it from the rocking curve used in ABI. We shall show in this paper how the measured TC may be used to perform quantitative phase imaging in a more general manner than our previously developed method.

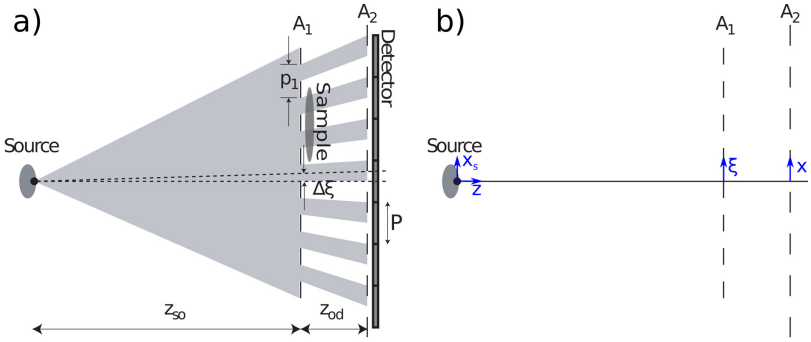

Fig. 1. Schematic diagram of a CAXPCI system which is not to scale (a) and specification of the coordinate systems used within this paper (b). The system is formed by two apertures A_1 and A_2. The sample is placed immediately after A_1. A_1 is translated by an amount $\Delta\xi$ in order to select the operating regime of the system. A_1 is placed a distance z_{so} from the source and A_2 is placed a distance z_{od} from A_1. The detector has pixels with a width of P and A_1 has a period of p_1. The distance along the optical axis is denoted z and is considered to begin at the centre of the source focal spot. The lateral dimensions within the source focal spot and within the planes of A_1 and A_2 are denoted x_s, ξ and x respectively. Each lateral dimension has its origin at the optical axis.

#181390 - $15.00 USD Received 7 Dec 2012; revised 11 Mar 2013; accepted 16 Mar 2013; published 30 Apr 2013

2. Theory

2.1. Derivation of expression for the translation curve

In this section we develop a forward model which allows the detector pixel signal to be calculated taking into account the salient system parameters. This formula is then used to obtain an expression for the TC of the system. We begin by mathematically defining the transmission function of the apertures as:

$$\mathscr{T}_i(x+nP) = \begin{cases} 1 & |x| < \eta_i P/2 \\ \exp(-\mu_{ca} T_i) & \text{otherwise} \end{cases}, \tag{1}$$

where the subscript i takes the value 1 or 2 in correspondence with the apertures A_1 and A_2 respectively. μ_{ca} is the energy dependent linear absorption coefficient of the absorbing material used to form the apertures (generally gold), T_i is the thickness of the absorbing material and η_i is the fraction of each aperture period which is non-absorbing. The sample is modelled by a multiplicative complex transparency function:

$$T(x) = \exp\left(-ik\phi(x) - \frac{1}{2}\int_{\mathscr{O}} \mu(x,z)\mathrm{d}z\right) \tag{2}$$

where μ is the linear absorption coefficient of the sample, k is the wave number, $\phi(x) = \int_{\mathscr{O}} \delta(x,z)\mathrm{d}z$, δ is the refractive index decrement of the sample and $\mathscr{O}$ is the extent of the sample. ϕ and μ both depend upon the photon energy, however, we develop the mathematical model by considering first a single energy before integrating over the source spectrum. Note also that the sample is assumed to satisfy the projection approximation, meaning that the sample is sufficiently thin and that inhomogeneities are large compared with the wavelength [19]. In this context, one criterion for being sufficiently thin is that the thickness is much less than z_{so} [20] although Paganin [21] presents a thorough discussion of this subject.

We now proceed to calculate the signal detected by each pixel assuming a monochromatic point source. We shall generalise to an extended, polychromatic source later. By applying the paraxial approximation to the Fresnel-Kirchhoff diffraction integral, we follow a previous publication [16] in evaluating the complex amplitude incident upon the detector aperture as

$$U(x) = C\int_{-\infty}^{\infty} \sqrt{\mathscr{T}_1(M(\xi-\Delta\xi))}T(\xi)\exp\left(ik\xi^2\frac{z_{so}+z_{od}}{2z_{so}z_{od}}\right)\exp\left(-ik\xi\frac{x}{z_{od}}\right)\mathrm{d}\xi \tag{3}$$

where

$$C = \frac{U_0}{\sqrt{i\lambda z_{so}z_{od}(z_{so}+z_{od})}}\exp\left(ik(z_{so}+z_{od})\right)\exp\left(ik\left(\frac{x^2}{2z_{od}}\right)\right) \tag{4}$$

and U_0 is defined implicitly by noting that the point source is assumed to emit a spherical wave, prior to applying the paraxial approximation, of the form $U_0\exp(ikr)/r$ where r is the distance from the source.

Without loss of generality, we consider the signal of the pixel bound by $|x| < P/2$. Then the signal detected by this pixel is given by

$$I = \int_{-P/2}^{P/2} \mathscr{T}_2(x)\,|U(x)|^2\,\mathrm{d}x \tag{5}$$

In order to simplify this expression into a more usable form, we approximate $T(x)$ as

$$T(x) \approx \tilde{T}(x) = \exp\left(-ik(\phi(0)+\phi_x(0)x) - \frac{1}{2}\int_{\mathscr{O}}\mu(0,z)\mathrm{d}z\right) \tag{6}$$

#181390 - $15.00 USD Received 7 Dec 2012; revised 11 Mar 2013; accepted 16 Mar 2013; published 30 Apr 2013

meaning that we assume that the object has a constant absorption and linear phase variation within the transmitting region of the pre-sample aperture. ϕ_x is thus the derivative of ϕ with respect to x and corresponds to the angle by which a ray is refracted by the sample. It is important to note that the coded aperture technique, like grating interferometry, measures refraction angle which, when multiplied by the wavenumber, yields the phase gradient. To avoid confusion arising due to the choice of wavenumber when employing a polychromatic source, we shall principally analyse refraction angle rather for the remainder of this paper.

In order to proceed, we substitute $\tilde{T}(x)$ for $T(x)$ into Eq. (3) and apply the stationary phase approximation in a manner similar to previous publications [16, 22]. The first order asymptotic solution to Eq. (3) is thus given by:

$$U^0(x) \sim U_0 \frac{\exp\left(ik(\mathrm{z_{so}}+\mathrm{z_{od}})\right)}{\mathrm{z_{so}}+\mathrm{z_{od}}} \exp\left(ik\left(\frac{x^2}{2\mathrm{z_{od}}}\right)\right) \exp\left(-\frac{1}{2}\int_{\mathscr{O}}\mu(0,z)\mathrm{d}z\right) \cdot \sqrt{\mathscr{T}_1\left(\mathrm{z_{od}}\phi_x(0)+x-M\Delta\xi\right)} \exp\left(-ik\frac{\mathrm{z_{so}}}{2\mathrm{z_{od}}(\mathrm{z_{so}}+\mathrm{z_{od}})}\left(\mathrm{z_{od}}\phi_x(0)+x\right)^2\right) \quad (7)$$

which may be substituted into Eq. (5) to obtain

$$I = \frac{|U_0|^2}{\left(\mathrm{z_{so}}+\mathrm{z_{od}}\right)^2} \exp\left(-\int_{\mathscr{O}}\mu(0,z)\mathrm{d}z\right) \int_{-P/2}^{P/2} \mathscr{T}_2(x)\,\mathscr{T}_1\left(\mathrm{z_{od}}\phi_x(0)+x-M\Delta\xi\right)\mathrm{d}x \quad (8)$$

Then, if the source focal spot is assumed to have a non-negative distribution, $S(x_s)$, at the target and the source spectrum and detector characteristics can be represented by a weighting $\sigma(E)$, the detector signal for an extended, polychromatic source may be obtained as [22]:

$$\begin{aligned} I &= \frac{|U_0|^2}{\left(\mathrm{z_{so}}+\mathrm{z_{od}}\right)^2} \int_{\text{spectrum}} \exp\left(-\int_{\mathscr{O}}\mu(0,z)\mathrm{d}z\right) \\ &\quad \cdot \int_{-P/2}^{P/2} \mathscr{T}_2(x)\left[\mathscr{T}_1\left(\mathrm{z_{od}}\phi_x(0)+x-M\Delta\xi\right) * S\left(x\frac{\mathrm{z_{so}}}{\mathrm{z_{od}}}\right)\right]\mathrm{d}x\sigma(E)\mathrm{d}E \end{aligned} \quad (9)$$

where $*$ is the convolution operator. We note that the convolution with S applies only to $\mathscr{T}_1$ since, formally, the argument x of $\mathscr{T}_1$ is written as $x + x_s\mathrm{z_{od}}/\mathrm{z_{so}}$ where x_s is a position within the source focal spot [22]. Since x_s only appears in the argument of $\mathscr{T}_1$, the convolution with S applies only to $\mathscr{T}_1$. As a final step, we note that it is possible to consider the polychromatic system as being equivalent to a monochromatic system at an equivalent or effective energy, to a good degree of accuracy [23]. We note also that this assumption was integral to one of the first demonstrations of quantitative phase imaging with polychromatic sources using a grating interferometer [11]. As a result we simplify Eq. (9) further to

$$I_P(\overline{\phi}_x,\overline{\mu},\Delta\xi) = \frac{|U_0|^2}{\left(\mathrm{z_{so}}+\mathrm{z_{od}}\right)^2} \exp\left(-\int_{\mathscr{O}}\overline{\mu}\mathrm{d}z\right) \int_{-P/2}^{P/2} \overline{\mathscr{T}}_2(x)\left[\overline{\mathscr{T}}_1\left(\mathrm{z_{od}}\overline{\phi}_x+x-M\Delta\xi\right) * S\left(x\frac{\mathrm{z_{so}}}{\mathrm{z_{od}}}\right)\right]\mathrm{d}x \quad (10)$$

where overlines have been added to the quantities above to denote that they are evaluated at the effective energy of the system. Furthermore, we have omitted the spatial dependence of $\overline{\mu}$ and $\overline{\phi}_x$ for brevity. We have now derived the key theoretical result of this paper. To further elucidate this result, consider Eq. (10) in the absence of a sample, which we write as:

$$I_{\mathrm{TC}}(\Delta\xi) = \frac{|U_0|^2}{\left(\mathrm{z_{so}}+\mathrm{z_{od}}\right)^2} \int_{-P/2}^{P/2} \overline{\mathscr{T}}_2(x)\left[\overline{\mathscr{T}}_1\left(x-M\Delta\xi\right) * S\left(x\frac{\mathrm{z_{so}}}{\mathrm{z_{od}}}\right)\right]\mathrm{d}x \quad (11)$$

#181390 - $15.00 USD Received 7 Dec 2012; revised 11 Mar 2013; accepted 16 Mar 2013; published 30 Apr 2013

where I_{TC} denotes the TC as it is obtained by translating the pre-sample aperture with respect to the detector aperture. We can then relate the pixel signal obtained with a sample in place to the TC as:

$$I_P(\overline{\phi}_x, \overline{\mu}, \Delta\xi) = \exp\left(-\int_{\mathscr{O}} \overline{\mu}\,\mathrm{d}z\right) I_{\mathrm{TC}}(\Delta\xi - \mathrm{z_{od}}\overline{\phi}_x/M), \tag{12}$$

from which we can derive inversion formulae for $\overline{\mu}$ and $\overline{\phi}_x$.

2.2. *Design of system parameters to enable quantitative imaging*

So far we have shown how a sample phase gradient, sample absorption and position of the pre-sample aperture affect the pixel signal. Now we show how this relationship may be inverted. Since we intend to determine two quantities, two measurements are required which correspond to different values of $\Delta\xi$, the values of which we now derive. Our strategy is to obtain two values of $\Delta\xi$ which will enable the absorption term to be factored out of Eq. (10). In particular, we acquire two images, I_1 and I_2 corresponding to two positions of the pre-sample aperture, $\Delta\xi_1$ and $\Delta\xi_2$ respectively. In order to extract the absorption term from sum of I_1 and I_2 we must thus find $\Delta\xi_1$ and $\Delta\xi_2$ which results in

$$F(\mathrm{z_{od}}\overline{\phi}_x(0)) = \int_{-P/2}^{P/2} \overline{\mathscr{T}}_2(x)\left[\left(\overline{\mathscr{T}}_1\left(\mathrm{z_{od}}\overline{\phi}_x(0)+x-M\Delta\xi_1\right)+\overline{\mathscr{T}}_1\left(\mathrm{z_{od}}\overline{\phi}_x(0)+x-M\Delta\xi_2\right)\right) * S\left(x\frac{\mathrm{z_{so}}}{\mathrm{z_{od}}}\right)\right]\mathrm{d}x \tag{13}$$

being approximately constant as $\mathrm{z_{od}}\overline{\phi}_x(0)$ varies. We thus seek values of $\Delta\xi_1$ and $\Delta\xi_2$ which minimises $|F'(\mathrm{z_{od}}\overline{\phi}_x(0))|$ everywhere. Within the domain $x \in [-P/2, P/2]$, $\overline{\mathscr{T}}_1{}'(x)$ is well approximated by $\overline{\mathscr{T}}_1{}'(x) = \delta(x+\eta_1 P/2) - \delta(x-\eta_1 P/2)$, where in this case, δ refers to Dirac's delta function. Thus our task reduces to minimising the expression:

$$\left|\int_{-P/2}^{P/2} \overline{\mathscr{T}}_2(x)\left[(\delta(\tilde{x}_1+\eta_1 P/2) - \delta(\tilde{x}_1-\eta_1 P/2) + \delta(\tilde{x}_2+\eta_1 P/2) - \delta(\tilde{x}_2-\eta_1 P/2)) * S\left(x\frac{\mathrm{z_{so}}}{\mathrm{z_{od}}}\right)\right]\mathrm{d}x\right| \tag{14}$$

where, for brevity, we have introduced $\tilde{x}_{1/2} = \mathrm{z_{od}}\overline{\phi}_x(0) + x - M\Delta\xi_{1/2} + \eta_1 P/2$. This expression cannot be made equal to zero in general. In order to proceed we assume only that $S(x_s)$ is symmetric about $x_s = 0$ and that it has its maximum value at $x_s = 0$. By noting that the convolution operator results in four shifted and scaled replicas of S, we select $\Delta\xi_1$ and $\Delta\xi_2$ such that two of them cancel and the other are shifted principally to where $\overline{\mathscr{T}}_2(x)$ has a small magnitude. The symmetry of these two criteria dictates a choice of $\Delta\xi_1 = -\Delta\xi_2$ and equating $-\delta(\tilde{x}_1 - \eta_1 P/2) + \delta(\tilde{x}_2 + \eta_1 P/2) = 0$ gives the result $\Delta\xi_2 = \eta_1 P/(2M) = \Delta\xi_0$ which is in agreement with our previous inversion technique [15] and thus defines the quantity $\Delta\xi_0$.

As a final step before deriving the inversion formulae we show that $|I_{\mathrm{TC}}{}'(\Delta\xi)|$ is maximised at $\Delta\xi = \pm\Delta\xi_0$. To proceed we note that $I_{\mathrm{TC}}{}'(\Delta\xi)$ is given by

$$I_{\mathrm{TC}}{}'(\Delta\xi) = \frac{-M|U_0|^2}{(\mathrm{z_{so}}+\mathrm{z_{od}})^2}\int_{-P/2}^{P/2} \overline{\mathscr{T}}_2(x)\left[S\left((x-M\Delta\xi+\eta_1 P/2)\frac{\mathrm{z_{so}}}{\mathrm{z_{od}}}\right) - S\left((x-M\Delta\xi-\eta_1 P/2)\frac{\mathrm{z_{so}}}{\mathrm{z_{od}}}\right)\right]\mathrm{d}x \tag{15}$$

Since we have not assumed a particular form of S, only that it is centred and maximised on $x_s = 0$, we conclude that $|I_{\mathrm{TC}}{}'(\Delta\xi)|$ is indeed maximised at $\Delta\xi = \pm\Delta\xi_0$ since this maximises the overlap between one of the S terms with the $\overline{\mathscr{T}}_2(x)$ term and minimises the overlap with the other.

#181390 - $15.00 USD Received 7 Dec 2012; revised 11 Mar 2013; accepted 16 Mar 2013; published 30 Apr 2013

2.3. Derivation of inversion formulae

We are now ready to derive the inversion formulae. In particular, we form images

$$\mathrm{I_L} = I_P(\overline{\phi}_x, \overline{\mu}, -\Delta\xi_0) = \exp\left(-\int_{\mathscr{O}} \overline{\mu}\,\mathrm{dz}\right) \mathrm{I_{TC}}\left(-\Delta\xi_0 - \mathrm{z_{od}}\overline{\phi}_x/M\right) \tag{16}$$

$$\mathrm{I_R} = I_P(\overline{\phi}_x, \overline{\mu}, \Delta\xi_0) = \exp\left(-\int_{\mathscr{O}} \overline{\mu}\,\mathrm{dz}\right) \mathrm{I_{TC}}\left(\Delta\xi_0 - \mathrm{z_{od}}\overline{\phi}_x/M\right). \tag{17}$$

In taking these measurements one must ensure that when the position of the pre-sample aperture is changed, the sample is also moved by an equivalent amount so that the same portion of the sample is within each X-ray beam. Alternatively, if the sample is scanned to improve spatial resolution, the left and right images must be co-registered. We now form the quantities:

$$\mathrm{I_\Sigma} = \mathrm{I_L} + \mathrm{I_R} = \exp\left(-\int_{\mathscr{O}} \overline{\mu}\,\mathrm{dz}\right) \left[\mathrm{I_{TC}}\left(-\Delta\xi_0 - \mathrm{z_{od}}\overline{\phi}_x/M\right) + \mathrm{I_{TC}}\left(\Delta\xi_0 - \mathrm{z_{od}}\overline{\phi}_x/M\right)\right] \tag{18}$$

$$\mathrm{I_\Delta} = \mathrm{I_L} - \mathrm{I_R} = \exp\left(-\int_{\mathscr{O}} \overline{\mu}\,\mathrm{dz}\right) \left[\mathrm{I_{TC}}\left(-\Delta\xi_0 - \mathrm{z_{od}}\overline{\phi}_x/M\right) - \mathrm{I_{TC}}\left(\Delta\xi_0 - \mathrm{z_{od}}\overline{\phi}_x/M\right)\right] \tag{19}$$

Furthermore, we now introduce some additional notation to distinguish between the reference TC and image data. In particular, from this point on we place hats on any image data from which phase and absorption will be retrieved. As shown previously, $\Delta\xi_0$ is chosen such that $\mathrm{I_{TC}}\left(-\Delta\xi_0 - \mathrm{z_{od}}\overline{\phi}_x/M\right) + \mathrm{I_{TC}}\left(\Delta\xi_0 - \mathrm{z_{od}}\overline{\phi}_x/M\right)$ is approximately constant, and thus approximately equal to $2\mathrm{I_{TC}}(\Delta\xi_0)$, which allows $\int_{\mathscr{O}} \overline{\mu}\,\mathrm{dz}$ to be found according to:

$$\int_{\mathscr{O}} \overline{\mu}\,\mathrm{dz} = \log\left[\frac{2\mathrm{I_{TC}}(\Delta\xi_0)}{\hat{\mathrm{I}}_\Sigma}\right]. \tag{20}$$

In order to derive the inversion formula for $\overline{\phi}_x$, we note that without making any further approximations, that the quantity $\hat{\mathrm{I}}_\Delta/\hat{\mathrm{I}}_\Sigma$ depends only upon $\Delta\xi_0$ and $\mathrm{z_{od}}\overline{\phi}_x$. We then form the function using the reference TC:

$$\begin{aligned} f: \quad \Omega_{\Delta\xi} &\to \Omega_{\mathrm{O}} \\ \Delta\xi_s &\mapsto \frac{\mathrm{I_{TC}}\left(-\Delta\xi_0 - \Delta\xi_s\right) - \mathrm{I_{TC}}\left(\Delta\xi_0 - \Delta\xi_s\right)}{\mathrm{I_{TC}}\left(-\Delta\xi_0 - \Delta\xi_s\right) + \mathrm{I_{TC}}\left(\Delta\xi_0 - \Delta\xi_s\right)} \end{aligned} \tag{21}$$

where $\Omega_{\Delta\xi} = [-a, a]$ for some positive real a, is chosen to ensure that f is injective. Then, any image data $\hat{\mathrm{I}}_\Delta/\hat{\mathrm{I}}_\Sigma$ with values within the range Ω_{O} can be related to a sample refraction angle, $\overline{\phi}_x$, by inverting f. This inversion technique is valid for a wider range of refraction angles than the existing CAXPCI inversion method. This is because the current method requires fewer assumptions and is based upon a single measured quantity, the TC.

It is, however, possible to obtain a linear inversion formula valid for smaller refraction angles. By expanding $\mathrm{I_R}$ and $\mathrm{I_L}$ in a Taylor series and again making the approximation $\mathrm{I_{TC}}\left(-\Delta\xi_0 - \mathrm{z_{od}}\overline{\phi}_x/M\right) + \mathrm{I_{TC}}\left(\Delta\xi_0 - \mathrm{z_{od}}\overline{\phi}_x/M\right) \approx 2\mathrm{I_{TC}}(\Delta\xi_0)$, gives

$$\begin{aligned} \frac{\mathrm{I_\Delta}}{\mathrm{I_\Sigma}} &\approx \frac{(\mathrm{z_{od}}\overline{\phi}_x/M)\mathrm{I'_{TC}}(\Delta\xi_0) - (\mathrm{z_{od}}\overline{\phi}_x/M)\mathrm{I'_{TC}}(-\Delta\xi_0) + O((\mathrm{z_{od}}\overline{\phi}_x)^3)}{2\mathrm{I_{TC}}(\Delta\xi_0)} \\ &= \frac{\mathrm{z_{od}}\overline{\phi}_x}{M}\frac{\mathrm{I'_{TC}}(\Delta\xi_0)}{\mathrm{I_{TC}}(\Delta\xi_0)} \end{aligned} \tag{22}$$

#181390 - $15.00 USD Received 7 Dec 2012; revised 11 Mar 2013; accepted 16 Mar 2013; published 30 Apr 2013

where the remainder term in the numerator is of third order because the second derivative of I_{TC} is approximately zero in the vicinity of $\Delta\xi_0$, since it was shown that the first derivative of I_{TC} is minimised at $\Delta\xi_0$. Eq. (22) can then be manipulated to reveal the sample refraction angle image as:

$$\overline{\phi}_x = \frac{M}{z_{od}} \frac{\hat{I}_\Delta}{\hat{I}_\Sigma} \frac{I_{TC}(\Delta\xi_0)}{I'_{TC}(\Delta\xi_0)} \tag{23}$$

where $I_{TC}(\Delta\xi_0)/I'_{TC}(\Delta\xi_0)$ is known from the experimentally measured TC.

3. Experimental example

The TC of the system is measured routinely whenever the pre-sample aperture is aligned with the detector aperture. An experimentally acquired TC is plotted in Fig. 2 using our laboratory CAXPCI system which has system parameters $z_{so} \approx$1.6m and $z_{od} \approx$0.4m. These quantities are approximate since the apertures and detector are initially placed in these positions and an alignment procedure is used to accurately position them. The pre-sample aperture, A_1, has period p_1=134μm and pixel width P=85μm. The detector aperture A_2 has a period of 83.5μm to allow it to be placed in front of the detector. The width of the transmitting regions of A_1 and A_2 are 16μm and 20μm respectively. The quantity $\Delta\xi$ refers to the displacement of A_1 from the position of perfect alignment with A_2. Note that in practice, every second pixel was skipped to minimise detector pixel cross talk. We employed a Rigaku 007HF X-ray tube generator operated at 35 kVp/25 mA with a rotating Mo target, an Anrad SMAM flat panel detector and the gratings were fabricated by Creatv Microtech (Potomac, Maryland, USA). The TC was acquired by taking the average over all pixels for each displacement of the pre-sample aperture. Note that the measured data points are unequally spaced as two separate measurements have been combined and one of the measurements was acquired only for negative values of $\Delta\xi$. The fitted curve was found by fitting a fourth order Fourier cosine series thus assuming symmetry about $\Delta\xi = 0$. We showed in Sec. (2.2) that $\Delta\xi_0$ should be chosen to be equal to half of the

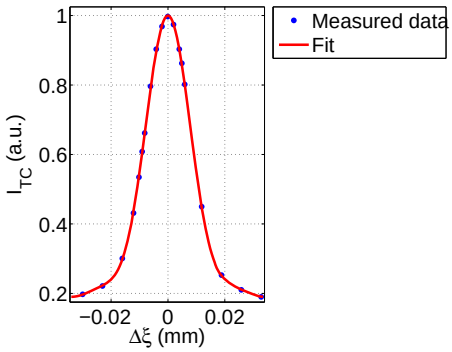

Fig. 2. Plot of experimentally acquired I_{TC}. The fitted curve was found by minimising the least square error with Fourier series containing four harmonic terms.

width of the transmitting region of the pre-sample aperture, which is 8μm in our experimental system. Figure 3 shows plots of I_L, I_R and I_Σ for the sampled TC which shows that I_Σ is indeed flat for a range of values of $\Delta\xi_s = z_{od}\overline{\phi}_x$. We can, however, show using the experimentally acquired TC, that the selected value of $\Delta\xi_0$ results in I_Σ being maximally flat over a range of

#181390 - $15.00 USD Received 7 Dec 2012; revised 11 Mar 2013; accepted 16 Mar 2013; published 30 Apr 2013

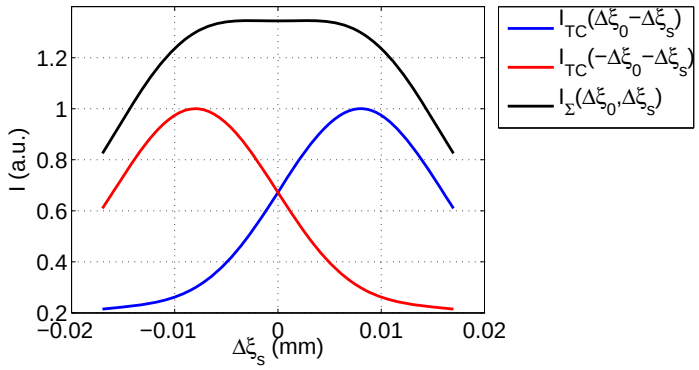

Fig. 3. Plot of $I_\Sigma = I_{TC}(-\Delta\xi_0 - \Delta\xi_s) + I_{TC}(\Delta\xi_0 - \Delta\xi_s)$, $I_{TC}(-\Delta\xi_0 - \Delta\xi_s)$ and $I_{TC}(\Delta\xi_0 - \Delta\xi_s)$ using the fitted TC plotted in Fig. 2.

values of $\Delta\xi_s$. In order to show this we define a measure of flatness as:

$$\varepsilon(\Delta\xi_0) = \frac{\max\limits_{\Delta\xi_s \in \Omega_{\Delta\xi_s}} (I_\Sigma(\Delta\xi_0, \Delta\xi_s)) - \min\limits_{\Delta\xi_s \in \Omega_{\Delta\xi_s}} (I_\Sigma(\Delta\xi_0, \Delta\xi_s))}{\text{mean}\limits_{\Delta\xi_s \in \Omega_{\Delta\xi_s}} (I_\Sigma(\Delta\xi_0, \Delta\xi_s))} \tag{24}$$

where $\Omega_{\Delta\xi_s} = [-5\times10^{-6}, 5\times10^{-6}]$ m was chosen to accommodate extreme values measured experimentally [16]. The maximum, minimum and mean values were found using the fitted TC. $\varepsilon(\Delta\xi_0)$ is plotted in Fig. 4 which shows that it exhibits a minimum value in the vicinity of $\Delta\xi_0$ as expected.

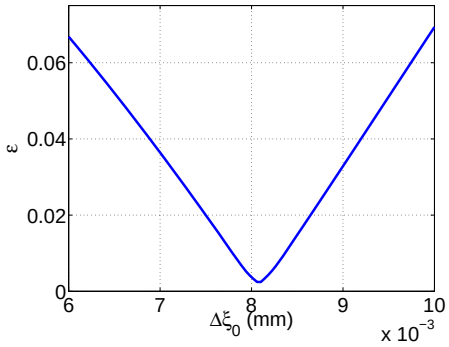

Fig. 4. Plot of $\varepsilon(\Delta\xi_0)$, a measure of the flatness of I_Σ for particular values of $\Delta\xi_0$ when $\Delta\xi_s$ takes values in the range $[-5\times10^{-6}, 5\times10^{-6}]$ m.

Another important factor which influences the choice of $\Delta\xi_0$ is the sensitivity to sample refraction angles. Figure 5 shows a plot of the derivative of the curve fitted to the experimentally observed TC data. This plot verifies the result obtained in Sec. (2.2), that the optimal values of the derivative of the TC appear in the vicinity of $\Delta\xi = \pm\Delta\xi_0$. A similar approach was employed by Diemoz *et al.* [24] for the case of grating interferometry. In particular, rather than phase stepping the detector grating, the pre-sample and detector gratings were offset by an amount which maximised the change in pixel signal for a given change to offset between the gratings. In their method, they make use of a principal analogous to the TC but, instead of separating

#181390 - $15.00 USD Received 7 Dec 2012; revised 11 Mar 2013; accepted 16 Mar 2013; published 30 Apr 2013

phase and absorption, obtain a single image containing a well described combination of phase and absorption information. This technique carries the advantage that a single acquisition is acquired per angle of rotation when performing CT imaging.

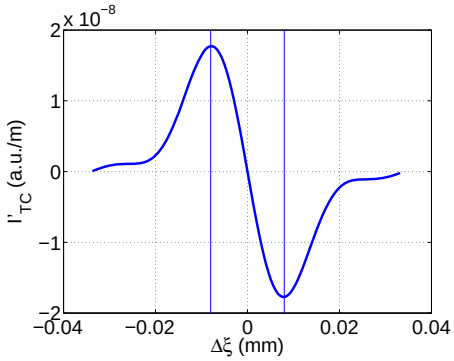

Fig. 5. Plot of the derivative of the fitted $I_{TC}(\Delta\xi)$, the vertical lines denote $\Delta\xi = \pm 8\mu$m.

The accuracy of Eq. (23) depends significantly on how constant the derivative of the TC is in the vicinity of $\Delta\xi_0$. Figure 6 shows how this derivative varies over a region which corresponds to a sample refraction angle satisfying $|\phi_x| < 10^{-5}$rad/m. The derivative of the rocking curve varies by at most approximately 15% over this range. Whilst this maximum error would be experienced only for extreme refraction angles, as explained in Sec. (2.3), it is possible to derive a refraction angle inversion formula without making such an assumption. Figure 7 shows a plot

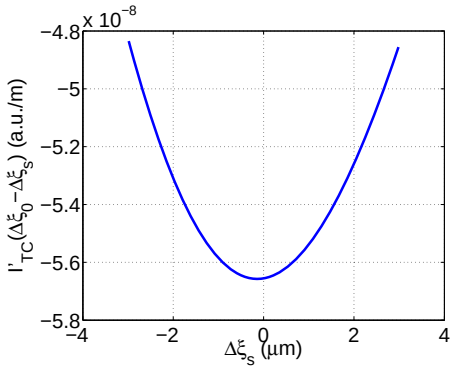

Fig. 6. Plot of $I_{TC}(\Delta\xi_0 - \Delta\xi_s)$ with $\Delta\xi_0 = 8\mu$m for a range of $\Delta\xi_s$ corresponding to $|\partial\overline{\phi}/\partial x| < 10^{-5}$rad/m.

of I_Δ/I_Σ versus $\Delta\xi_s$ for the experimental system being considered, using the fitted TC plotted in Fig. 2. The plot shows that, in order to uniquely determine $\Delta\xi_s$ from an observed value of $\hat{I}_\Delta/\hat{I}_\Sigma$, it is necessary to restrict the domain of $\Delta\xi_s$ to $|\Delta\xi_s| \lesssim 0.011$ mm which implicitly restricts the observable refraction angles to the range $|\overline{\phi}_x| \lesssim 0.034$ rad/mm. The refraction angle may be extracted from an observed value of $\hat{I}_\Delta/\hat{I}_\Sigma$ by numerically determining, from Fig. 7, the value of $\Delta\xi_s$ to which it corresponds. This numerical inversion may be performed very accurately and efficiently.

#181390 - $15.00 USD Received 7 Dec 2012; revised 11 Mar 2013; accepted 16 Mar 2013; published 30 Apr 2013

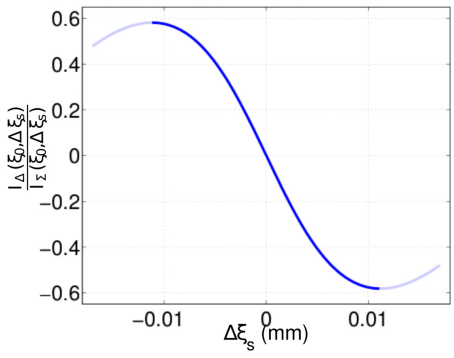

Fig. 7. Plot of I_Δ/I_Σ versus $\Delta\xi_s$. The domain of the plot is restricted to the non-shaded region so that there is a one-to-one mapping from $\Delta\xi_s$ to I_Δ/I_Σ. The plot was calculated using the fitted TC in Fig. 2.

4. Examples and analysis

In this section we analyse the TC refraction angle retrieval method and show some examples of how it may be applied. In particular, we show how the TC method differs from that previously published for the experimental system considered in Sec. (3) using some experimentally acquired images. We also perform some numerical simulations to demonstrate the improvement offered by the TC method.

We begin by comparing the TC refraction angle extraction algorithm with that published previously, derived analytically and based upon the assumption of perfectly absorbing apertures. In particular, we have previously published [15] a phase extraction algorithm which extracts the refraction angle according to the formula:

$$\overline{\phi}_x = -\mathrm{erf}^{-1}\left(\frac{\hat{I}_\Delta}{\hat{I}_\Sigma}\right)\frac{\sigma_d}{z_{od}} \tag{25}$$

$$\approx -\frac{\sqrt{\pi}}{2}\frac{\hat{I}_\Delta}{\hat{I}_\Sigma}\frac{\sigma_d}{z_{od}} \tag{26}$$

where erf is the standard error function $\mathrm{erf}(z) = 2/\sqrt{\pi}\int_0^z \exp(-t^2)\mathrm{d}t$ and $\sigma_d = \mathrm{FWHM}_d/\left(2\sqrt{\log(2)}\right)$ and FWHM_d is the full width at half maximum of the beams projected onto the detector aperture. Figure 8 shows a comparison between the analytic inversion formulae and those obtained using the TC plotted in Fig. 7. All of the plots relate to the system used to obtain the TC plotted in Fig. 2. σ_d was found to be approximately 12.5μm by determining the focal spot size which gave the best match between calculated and measured TCs. The TC approach should, in general, predict a refraction angle greater or equal in magnitude compared with the analytic method, since the TC method implicitly takes account of the partial absorption by the apertures.

The refraction angle retrieval curves in Fig. 8 reveal that the full and approximate TC methods are equivalent for small refraction angles yet diverge strongly for large refraction angles. This will lead to the approximate TC method underestimating refraction angles. This phenomenon results from the partial transmission of X-rays through the apertures as is demonstrated by the remaining plots in Fig. 8. In particular, the full analytic method (Eq. (25)) and the ideal TC methods coincide. The ideal TC inversion curve was obtained from a simulated TC for the case of perfectly absorbing apertures. The approximate analytic curve (Eq. (26)) departs

#181390 - $15.00 USD Received 7 Dec 2012; revised 11 Mar 2013; accepted 16 Mar 2013; published 30 Apr 2013

only slightly from the full analytic curve.

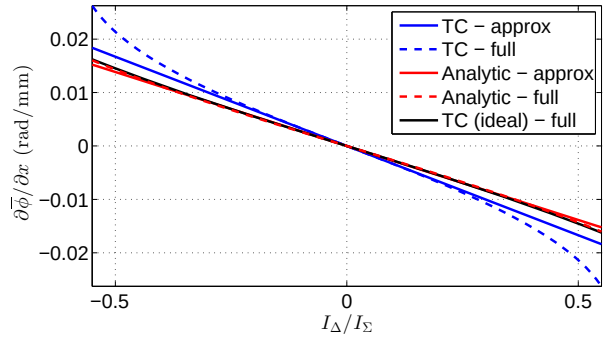

Fig. 8. Comparison of the inversion formulae. TC-approx is described by Eq. (23), TC-full by inverting Eq. (21) using the experimental TC in Fig. 2, Analytic-approx by Eq. (26) and Analytic-full by Eq. (25), TC (ideal)-full is found using an ideal TC, calculated assuming fully absorbing apertures.

We now present an example showing how three of the refraction angle inversion relationships in Fig. 8 result in different values of refraction angle in an experimental case. We used the experimental system for which the TC in Fig. 2 was obtained, to image a titanium wire of radius 125μm. Images were taken at a total of 16 sub-pixel object positions in order to increase spatial resolution. Each such image had an 8.75 second exposure time. We selected this sample due to its very high value of δ throughout the source spectrum, even though it is also highly absorbing. High values of δ causes high values of $|\hat{\mathrm{I}}_\Delta/\hat{\mathrm{I}}_\Sigma|$ to be measured which is where the greatest difference between the three inversion formulae occurs. We have also shown, for reference, the theoretical refraction angle at the estimated mean energy of the spectrum (18keV). We do not expect the experimentally acquired results to match this profile due to beam hardening which results from absorption by the wire [25]. The main point of these plots is to show an experimental case where the full TC inversion formula is required for accuracy in order to account for large refraction angles. This difference arises because the linearity of the TC breaks down for large separations between the pre-sample and detector apertures. We also imaged aluminium, sapphire, polyetheretherketone and boron wires but these samples did not result in a difference between the full and approximate TC refraction angles. The expected refraction angle in Fig. 9 can only be calculated with accurate knowledge of the source and detector spectral responses and the sample absorption [25]. In light of this and in order to further demonstrate the advantages of the TC inversion method we now present some numerical simulations.

We modelled the experimental system considered in Sec. (3) using an estimated spectrum as plotted in Fig. 10 and assuming that the Anrad SMAM flat panel detector is energy integrating with photon weighting directly proportional to photon energy. We also assumed that the source has a focal spot with a FWHM of 60μm. All other system parameters are as described in Sec. (3). We considered a polyetheretherketone (PEEK) fiber of radius 100μm, assumed to have chemical composition $C_{19}O_3H_{18}$ and density 1.3 gm/cm^3. The refractive index data was obtained theoretically [26] which is also plotted in Fig. 10. Note that we use β to refer to the imaginary part of refractive index. The refractive index for the gold apertures was also calculated from theory [26]. The simulation method is described fully in previous publications [17, 22] however it takes as its starting point Eq. (3) which is evaluated numerically for a range of photon energies within the spectrum. The values of T and $\mathscr{T}_1$ are calculated according to photon energy. As such, the simulation is accurate to within the approximations of the paraxial Fresnel-Kirchhoff diffraction integral and the projection approximation as discussed in

#181390 - $15.00 USD Received 7 Dec 2012; revised 11 Mar 2013; accepted 16 Mar 2013; published 30 Apr 2013

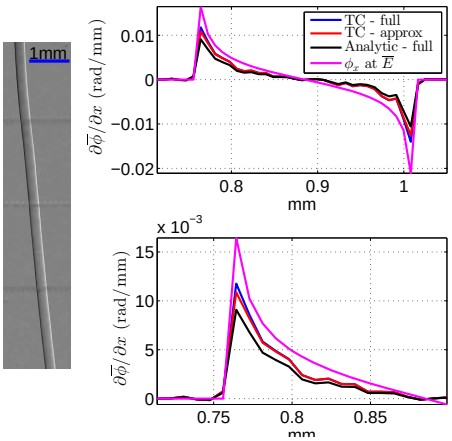

Fig. 9. (left) an image of I_Δ/I_Σ for a 125μm titanium wire, (top right) line profiles of $\overline{\phi}_x$ through the titanium wire and (bottom right) a zoomed in version of the top right plots. Line profiles were calculated using the three inversion formula indicated by the legend. $\overline{E}$ is the estimated mean energy of the spectrum and ϕ_x at $\overline{E}$ is the theoretical value of ϕ_x at the mean energy.

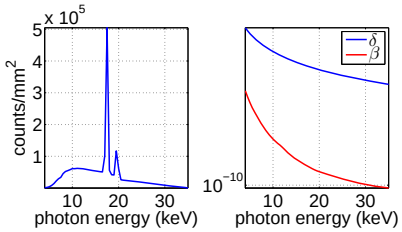

Fig. 10. Plots of the source spectrum (left) and refractive index of PEEK (right) as employed in the simulation.

Sec. (2.1). Each refraction angle was calculated at 51 sample points by scanning the object to increase spatial resolution. This was only for the purposes of numerical comparison, to ensure that the integrated refraction angle did not experience artefacts resulting from the integration.

We have performed simulations for both the polychromatic and monochromatic cases, however, assuming a 60μm FWHM focal spot in both cases. The monochromatic simulation serves to demonstrate that the TC technique performs very accurate quantitative phase retrieval in a scenario when phase is well defined. When a polychromatic source is employed, the concept of phase is ambiguous since it implies an averaging of phase. Furthermore, any such measured phase will depend on the source, aperture, detector and sample spectral properties [25].

Figure 11(a) shows the calculated TC for the polychromatic case for aperture gold thicknesses of 10, 20, 40 and 80μm respectively. We note that no significant variation in calculated TC or retrieved refraction angle was observed for aperture gold thicknesses exceeding 80μm. Figure 11(b) shows the calculated TC for the monochromatic case at the spectrum mean energy of 18keV. The two simulations assume the same source power density. Figure 11(c) shows the refraction angle retrieval relationship, Eq. (21), corresponding to the polychromatic TCs of Fig. 11a) and Fig. 11(d) shows the retrieval relationship corresponding to the monochromatic TCs of Fig. 11b). The two cases are similar, but not identical. In particular, we note that in the polychromatic case, thicker gold is required to achieve the ideal refraction angle relationship where

#181390 - $15.00 USD Received 7 Dec 2012; revised 11 Mar 2013; accepted 16 Mar 2013; published 30 Apr 2013

there is insignificant transmission through the apertures.

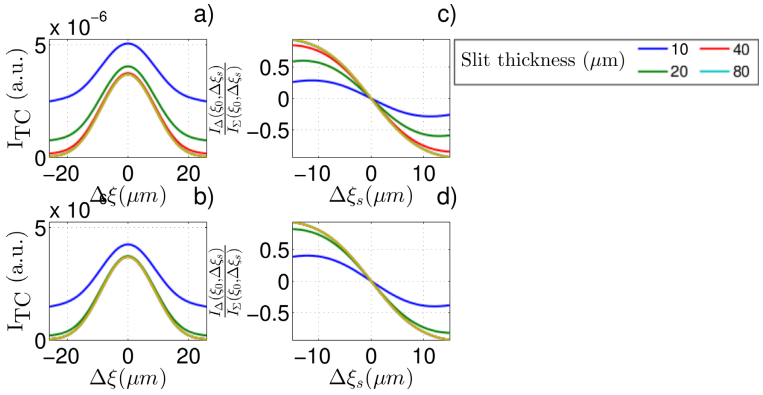

Fig. 11. Plots of the translation and inversion curves for the four aperture thicknesses employed which are indicated in the legend. Plots a) and c) correspond to the polychromatic case whilst plots b) and d) correspond to the monochromatic case at the spectrum mean energy of 18keV.

We first explain how the numerical results are analysed. As previously discussed, the system results in a measurement of refraction angle, $\overline{\phi}_x$. In this example we consider the object to have a circular cross section and so within the support of the object, $\overline{\phi}$ is given by $\overline{\phi} = 2\overline{\delta}\sqrt{R^2 - x^2}$ where, as usual, overlines are used to denote quantities averaged over the spectrum. Spatial variation is thus contained within the function which describes the shape of the object. In what follows, we plot the integrated refraction angle, $\overline{\phi} = \int \overline{\phi}_x \mathrm{d}x$ which enables $\overline{\delta}$ to be determined since the shape function is known. The integrated refraction angle can be used to obtain an measurement of integrated phase through multiplication by an effective wavenumber.

Figure 12 shows the integrated refraction angle for the polychromatic ((a) and (c)) and monochromatic ((b) and (d)) cases and using the TC refraction angle retrieval ((a) and (b)) and the approximate linear method Eq. (26) ((c) and (d)). The integrated refraction angle, calculated analytically, at the spectrum mean energy has also been plotted. We note that only in case b) do all integrated refraction angles match the analytic profile. Agreement should be expected in this case since it has not been necessary to assume the existence of an effective energy for the spectrum in order to obtain Eq. (10). In both c) and d), the approximate linear method results in a large variation between measured integrated refraction angle for the different aperture thicknesses, although we note that in the monochromatic case, the solution is very close to the analytic case for the 80μm thick apertures. Both the approximate linear cases exhibit wide variation simply because the method doesn't take into account X-ray transmission through the apertures. The polychromatic case returns a generally greater phase change than the monochromatic simply because the average value of δ across the spectrum is greater than δ at the mean energy of the spectrum. The plots in Fig. 12(a), however, demonstrate the main result of this paper. Here we see a much smaller variation in the integrated refraction angle as aperture thickness varies. This shows that the TC method reduces the impact of the system's spectral properties on the measured refraction angle. In order to more thoroughly analyse the results plotted in a) we present the values of $\overline{\delta}$ measured for each aperture thickness in Table 1. We expect the predicted value of $\overline{\delta}$ to converge towards the value of δ averaged over the spectrum, ie, $\delta_{ave} = \int \delta(E)\sigma(E)\mathrm{d}E = 1.16 \times 10^{-6}$. Whilst this value is within the range of predicted values of $\overline{\delta}$, the values do not converge to this value. This error arises due to the approximation that the system has an effective energy made in order to simplify Eq. (9) to Eq. (10).

#181390 - $15.00 USD Received 7 Dec 2012; revised 11 Mar 2013; accepted 16 Mar 2013; published 30 Apr 2013

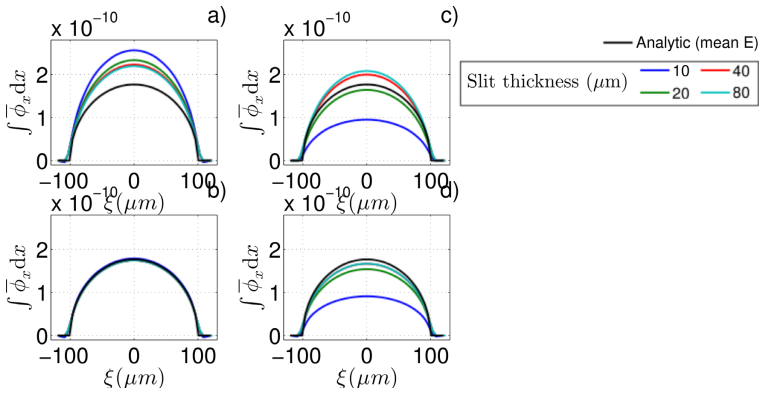

Fig. 12. Plots of integrated refraction angle across the simulated PEEK fiber of 100μm radius. Plot a) and c) correspond to the polychromatic case whilst plots b) and d) correspond to the monochromatic case at the spectrum mean energy of 18keV. Plots a) and b) have been obtained using the TC inversion technique whilst plots c) and d) have been obtained using the linear approximation. The analytic sample phase at the spectrum mean energy has been plotted on all axes for reference.

Table 1. Numerically determined values of $\overline{\delta}$ for four different values of aperture gold thickness. $\overline{E}_{\overline{\delta}}$ is the photon energy at which PEEK has $\delta = \overline{\delta}$.

Gold thickness (μm)	$\overline{\delta} \times 10^6$	$\overline{E}_{\overline{\delta}}$(keV)
10	1.28	15.0
20	1.17	15.7
40	1.12	16.0
80	1.10	16.2

5. Conclusions

We have demonstrated a new quantitative technique for measuring X-ray refraction angle and absorption using the coded aperture method with a laboratory source. The quantitative technique requires knowledge of only the so-called translation curve which is obtained by recording the detector signal as the pre-sample aperture is translated relative to the detector aperture. The translation curve is measured routinely when the system is aligned.

We showed that the new technique is more accurate for measuring larger refraction angles and also is more accurate in the case where the apertures are only partially absorbing. We compared the new technique with that previously used which assumed that the apertures were perfectly absorbing. We showed that the new method is significantly more accurate in the case of partially absorbing apertures. Finally, we showed that the proposed technique measures an average value of refraction angle based upon the sample's value of δ averaged over the spectrum, rather than, for example, measuring δ at the average energy of the spectrum.

Acknowledgments

This work was funded by the UK Engineering and Physical Sciences Research Council (EP/G004250/1 and EP/I021884/1). P.M. is currently supported by a Discovery Early Career Research Award from the Australian Research Council (DE120101331).

#181390 - $15.00 USD Received 7 Dec 2012; revised 11 Mar 2013; accepted 16 Mar 2013; published 30 Apr 2013